Influence of the temperature on the reduction mechanism of concentrated nitric acid on a silicon-enriched austenitic stainless steel

I. Bahtit, N. Gruet, B. Puga, X.R. Nóvoa, Cyril Thomas, V. Vivier

Influence of the temperature on the reduction mechanism of concentrated nitric acid on a silicon-enriched austenitic stainless steel

I. Bahtit,[1,2] N. Gruet,[2,*] B. Puga,[2,*] R. Novoa,[3] C. Thomas,[1] V. Vivier[1]

[1]Sorbonne Université, CNRS, Laboratoire de Réactivité de Surface (LRS), 4 place Jussieu, F-75005, Paris, France

[2]Université Paris-Saclay, CEA, Service de la Corrosion et du Comportement des Matériaux dans leur Environnement, F-91191, Gif-sur-Yvette, France

[3]CINTECX, Universidade de Vigo, ENCOMAT Group, EEI, Campus Universitario, 36310 Vigo, Spain

*corresponding authors: nathalie.gruet@cea.fr (N. Gruet); beatriz.puga@cea.fr (B. Puga)

Abstract

Corrosion of silicon-enriched stainless steel in nitric acid strongly depends on the temperature of the electrolyte. Therefore, the reduction reaction of nitric acid on this material was investigated from 40 to 107 °C. For the first time, the autocatalytic reduction mechanism of nitric acid reduction is highlighted by coupling electrochemical measurements (LSW, EIS, Chronoamperometry) with chemical analyses (mass spectrometry, ICP-AES, UV-Vis spectroscopy). This study provides further insights into the nitric acid reduction on an oxidized material compared to that reported earlier on noble metals despite slower kinetics of electrochemical reactions due to the presence of a passivating film. Furthermore, it is shown that HNO_2 (or NO^+) promotes the autocatalytic reactions in concentrated HNO_3 and leads to the formation of NO_x species released and detected in the gas phase.

Keywords: Autocatalytic mechanism; Electrochemical measurements; Mass Spectrometry; reduction; Stainless steel

1. Introduction

Concentrated nitric acid media, known to be corrosive electrolytes, are commonly used for different applications such as the oxidation of carbon nanotubes [1,2], the dissolution of materials for ICP analysis [3] or the dissolution of spent nuclear fuels [4]. For some of these applications, stainless steels (SS) are mainly used for their high resistance to these oxidizing environments. Therefore, a comprehensive understanding of the physicochemical properties of the electrolyte is of the utmost importance to prevent damage to the metallic structure. For instance, the temperature at which the electrolyte (concentrated acid nitric) is used can promote the corrosion rate of stainless steel to a significant extent [5,6].

Concentrated nitric acid is a complex medium involving various nitrogen species in the liquid and gas phases. Therefore, many works have been devoted to the study of the reduction mechanism of nitric acid on inert metals [7–16]. All these works have concluded the existence of an autocatalytic mechanism for which HNO_3 is not considered an autocatalytic species. Additionally, the complex autocatalytic mechanism is sensitive to nitric acid concentration [14] and the electrode potential [13].

About 60 years ago, Vetter [10,16] and Schmid et al. [7–9] independently proposed reduction mechanisms on platinum for nitric acid concentrations in the range of 1 to 10 mol L^{-1} at 20 °C. Later, Razygraev et al. [11,12] performed experiments in 2 mol L^{-1} boiling nitric acid, showing that both of the proposed previous mechanisms [3-6] may occur, but at different cathodic overpotentials. These results were subsequently confirmed by Sicsic *et al.* [13] through experimental work performed in 4 mol L^{-1} nitric acid solution at 40 °C on platinum and gold electrodes. From these works, the two mechanisms can be summarized as follows:

- The Vetter's mechanism takes place within a 0.85 V/SHE < E < 1.15 V/SHE potential range [6]. In this mechanism, NO_2 (+4 nitrogen oxidation state) is assumed to be the

main electroactive species. Its generation (Eq(2) occurs at the electrode with slow heterogeneous kinetics.

$$NO^{+}_{(ads)} + NO_3{}^{-}_{(ads)} \longleftrightarrow N_2O_{4\,(ads)} \quad (1)$$

$$N_2O_{4(ads)} \longleftrightarrow 2NO_{2\,(ads)} \quad (2)$$

$$NO_{2\,(ads)} + e^{-} \longleftrightarrow NO_2{}^{-}_{(ads)} \quad (3)$$

$$NO_2{}^{-}_{(ads)} + H^{+} \longleftrightarrow HNO_{2\,(ads)} \quad (4)$$

$$HNO_{2\,(ads)} + H^{+} \longleftrightarrow NO^{+}_{(ads)} + H_2O_{(l)} \quad (5)$$

- Schmid's mechanism takes place within a 0.65 V/SHE < *E* < 0.85 V/SHE potential range [7–9] lower than that of Vetter [10,16]. In this case, a homogeneous mechanism involving HNO_2 or NO^+ (+3 nitrogen oxidation state) as the electroactive species is occurring. The latter species is generated in a reaction layer in solution near the electrode (Eq. *(6*) and not at the surface of the electrode as is the case in Vetter's mechanism (Eq. *(5*). The Schmid's mechanism is supported by the evolution of the current/voltage curve as a function of the rotation rate of a rotating disk electrode (RDE). The lowest currents are measured at the highest rotation rate, a high rotation rate driving the active species away from the vicinity of the electrode. The following mechanism was thus proposed:

$$2HNO_{2(aq)} + 2H^{+}_{(aq)} \longleftrightarrow 2NO^{+}_{(aq)} + 2H_2O_{(l)} \quad (6)$$

$$2NO^{+}_{(aq)} \longleftrightarrow 2NO^{+}_{(ads)} \quad (7)$$

$$2NO^{+}_{(ads)} + 2e^{-} \longleftrightarrow 2NO_{(ads)} \quad (8)$$

$$2NO_{(ads)} \longleftrightarrow 2NO_{(aq)} \quad (9)$$

$$2NO_{(aq)} + HNO_{3(aq)} + H_2O \longleftrightarrow 3HNO_{2(aq)} \quad (10)$$

Below 0.65 V/SHE, the autocatalytic cycle is interrupted by the reduction reaction of NO into N_2O (Eq. *(11)*, which results in a significant decrease (in absolute value) of the cathodic current density.

$$2NO_{(ads)} + 2H^+_{(aq)} + 2e^- \longleftrightarrow N_2O_{(ads)} + H_2 \qquad (11)$$

Nevertheless, the nitric acid electrolyte remains a medium of great complexity in which reactions are difficult to predict accurately due to multiple parameters. Despite different temperature conditions that have been studied in earlier studies, the influence of temperature on nitric acid reduction is still not comprehensively understood. Some authors have simulated the evolution of the different nitrogen species with the temperature [17]. In particular, it has been shown that an increase in temperature favoured the formation of undissociated HNO_3 (decrease in H^+ and NO_3^- concentrations) and the production of some gaseous species such as NO and NO_2. In contrast, such an increase in temperature decreased the stability/concentration of HNO_2. Finally, the redox potential of the solution was reported to increase as the temperature increased, making the medium more oxidizing. We can assume that all these parameters directly impact on the kinetics of the reactions involved in the reduction of nitric acid.

In the case of a stainless steel electrode, the reaction mechanism at the metal/solution interface is even more complex to be unravelled since the reaction kinetics are slowed down by the presence of a passivating layer at the metal surface [18]. Razygraev et al. [19] have studied the temperature dependence of nitric acid reduction on various materials and have suggested that some reactions may be inhibited depending on the surface type. However, these authors have also indicated that both Schmid's and Vetter's mechanisms would compete and occur at higher overpotentials to compensate for slow kinetics. Benoit [20] and Balbaud et al. [21] have also proposed a nitric acid reduction mechanism based on Schmid's findings

to account for the results obtained in 4 and 8 mol L^{-1} nitric acid solutions at 40 and 100 °C, respectively. These authors also claimed that the slow cathodic kinetics inhibited the autocatalytic step of the mechanism due to the slow build-up of catalytic species in the close vicinity of the electrode surface (i.e., in the reaction layer). Balbaud et al. have also shown that the current density was sensitive to the rotation rate of the stainless-steel electrode at -0.4 V/MSE in 4 mol L^{-1} HNO_3 at 25 °C [15], in agreement with Schmid's mechanism proposal. In contrast, Benoit et al. [20] did not report on any influence of the rotation rate on the current densities in the course of experiments performed on a 304L stainless steel rotating disk electrode in 4 and 8 mol L^{-1} nitric acid solutions at 40 and 100 °C, respectively, between 0.3 and -0.25 V/MSE.

To better understand the role of the temperature on the abovementioned mechanisms, the present work reports on the development of an electrochemical set-up coupled to gas phase analysis by mass spectrometry (EC-MS) adapted for the study of the reduction mechanism on stainless steel of hot concentrated nitric acid (80 and 107 °C, the latter temperature corresponding to the boiling temperature of HNO_3). In parallel, nitrous acid and dissolved iron concentrations were recorded over time, while cathodic overpotentials were applied, using a colorimetric analysis and an ICP-AES technique, respectively. Finally, the results are discussed and compared to earlier literature data to propose a model that accounts for the reactivity of a passive electrode in highly concentrated nitric acid solutions at high temperatures.

2. Experimental

2.1. Material

The material studied in this work is silicon-enriched stainless steel (X1 Cr-Ni-Si 18-15-4). The chemical analysis of this material (**Table 1**) was performed using glow discharge optical emission spectroscopy (GD-OES) with a GD-Profiler from Horiba Jobin-Yvon.

Two different samples were used as working electrodes for the electrochemical measurements: a bullet-shaped (2 cm^2) and a rectangular (18 cm^2) electrode. These electrodes were first electropolished in a 96% H_2SO_4 / 85% H_3PO_4 (50/50) mixture for approximately 30 min before being rinsed and cleaned successively with ethanol and acetone in an ultrasonic bath to remove the strain-hardening layer and to have the same initial surface and roughness (Ra) of working electrodes. For all measurements, the silicon-enriched stainless steel undergoes a relatively homogeneous dissolution.

Table 1: Chemical composition (wt%) of the silicon-enriched stainless-steel sample.

	Fe	**Cr**	**Ni**	**Si**	**Mn**	**Mo**
X1 Cr-Ni-Si 18-15-4	60.67	17.76	15.51	4.17	1.60	0.29

2.2. Chemicals

All experiments were performed in 2.5 mol L^{-1} HNO_3 and 2.5 mol L^{-1} $NaNO_3$ solutions prepared from concentrated nitric acid solution (52.6%, Sigma Aldrich) and sodium nitrate salt (99.6%, Sigma Aldrich) in deionized water (18.2 MΩ.cm) obtained from a Millipore distillation unit.

2.3. Electrochemical measurements

A three-electrodes set-up was used for this electrochemical study. The reference electrode (REF) and the counter electrode (CE) were a mercury/mercurous sulfate electrode (Hg/Hg_2SO_4: MSE, E = +0.65 V/SHE at 25 °C) and a platinum grid, respectively. The

working electrode was made of X1 Cr-Ni-Si 18-15-4 stainless steel. All the experiments were performed with a VSP workstation (Biologic) controlled by an EC-lab v.10.36 software.

Cathodic polarization curves were recorded with a low scan rate of potential (0.2 mV s^{-1}) from E_{corr}+0.030 V/MSE after about 72 h of stabilization time.

Before electrochemical impedance spectroscopy (EIS) measurements for the different cathodic potentials (-0.2, -0.3 and -0.4 V/MSE), chronoamperometry was performed to ensure a steady-state current. EIS spectra were measured in two sequences on a wide frequency range: From 100 kHz to 10 mHz with 10 mV amplitude and then from 10 to 1 mHz with 20 mV amplitude. This configuration fulfils measurements' linearity requirements and minimises the noise in the impedance response. All the EIS spectra were submitted to the Kramers-Kronig test to verify linearity [22].

2.4.Mass spectrometry

Gas analysis was performed using an Omnistar mass spectrometer (Pfeiffer) with a channeltron detector. Mass-to-charge ratios (m/z) were recorded over time: 30, 44 and 46, corresponding to NO, N_2O and NO_2, respectively. The data are plotted as ionic current and time evolution for each gaseous species.

2.5. Inductively coupled plasma atomic emission spectroscopy (ICP-AES)

ICP-AES analyses were performed with a SpectroBlue (Ametek) after collecting a small volume (3 ml) of nitric acid solution allowing the concentration of dissolved iron to be determined as a function of the applied potential.

2.6. Griess analysis

Quantitative analysis of nitrous acid was performed using a GRIESS-ILOSVAY'S nitrite reagent from Merck KGaA. During chronoamperometry measurements, a small volume of

nitric acid (< 2 ml) was collected in the reactor and mixed with the Griess reactant. After several hours, a pink colouration can be obtained, and its maximum absorbance at 530 nm was measured using a UV-visible spectrometer (Cary 50, VARIAN). In the case of significant amounts of nitrites, an additional dilution of the sample was carried out to match the concentration range of the pre-established calibration curve. The HNO_2 concentration in the reactor was deduced from the calibration curve within a range of concentrations of 0.5 to 2.5 x 10^{-5} mol L^{-1} and the dilution factor.

3. Results and Discussion

3.1. Effect of the temperature on the electrochemical behavior of the silicon-enriched stainless steel in nitric acid

3.1.1. Evolution of cathodic currents as a function of temperature

Polarization curves of the stainless steel recorded at 40, 60, 80 and 107 °C in nitric acid solution are shown in **Figure 1** (it was chosen to present only the cathodic branch of the polarization curves since the discussion is related to the reduction mechanism of nitric acid). The cathodic traces (full lines) show a decrease in the corrosion potential (E_{corr}) when the temperature increases. A shift to higher potentials is generally expected as the medium becomes more oxidizing with increasing temperature, as observed by Hasegawa on a 304L stainless-steel sample [23]. These authors reported a significant increase in the cathodic current compared to the anodic current, responsible for a shift of the corrosion potential towards higher potentials.

The cathodic current appears to be increasing as the temperature increases, and the slope of the current/potential curve changes significantly between 60 and 80 °C, which can be ascribed not only to a change in the reaction kinetics but also to a change in the reduction mechanism.

For potentials lower than E_{corr}, the anodic current related to the oxidation of the material is screened by the cathodic current. Therefore, the measurement does not capture the boundaries of stainless steel's passive and active regions. However, at low potentials (for example, around -0.55 V/MSE at 80 °C, **Figure 1**), a sharp increase in the cathodic current can be seen and ascribed to the beginning of the active domain of stainless steel, which modifies its surface reactivity. Under such conditions, the oxide layer does not play its protective role as it does in the passive domain. Electron transfer is enhanced, consequently amplifying faradaic reactions and the cathodic current.

An approximate active/passive transition potential, E_{act}, can be estimated graphically from **Figure 1** with the intersection of two tangents (one set on the first current-potential slope below E_{corr} and the other one set on the vertical current-potential slope at the lowest potentials displayed in **Figure 1**). Therefore, E_{act} is located near the bottom of the current wall at the low potentials. **Figure 2** plots the estimated values of E_{act} as a function of the temperature. The evolution of E_{act} as a function of the temperature (slope of 0.027 V K^{-1}) is found to agree with that reported earlier by Laurent, which was obtained in 4 mol L^{-1} nitric acid solution from 28 to 80 °C and using an electrochemical measurement coupled with a plasma atomic emission spectrometer technique (AESEC) for the determination of E_{act} of the X1 Cr-Ni-Si 18-15-4 SS [24]. However, a slightly higher value of E_{act} was determined in the present study compared to Laurent's [24]. This slight discrepancy can be attributed to differences in the two methods used for E_{act} determination (Graphical in the present work and AESEC in ref. [24]) and/or experimental conditions.

Steady-state measurement of the current performed by chronoamperometry at various potentials for the same temperature range, also plotted in **Figure 1** (symbols), correlate with those obtained from a linear scan of the potentials at a low scan rate for potentials between that of corrosion and -0.3 V/MSE. For lower potentials (**Figure 1**), the steady-state currents

are higher, except at 107 °C, than those obtained dynamically, which indicates a change of the mechanism involving a determining step corresponding to the activation of nitric acid reduction through an autocatalytic mechanism. Whereas the cathodic current of a long-time polarization experiment performed at -0.4 V/MSE and 80 °C appears to reach steady-state after about 2 h (**Figure 3**, green trace), this is not the case for the same experiment carried out at 107 °C (**Figure 3**, red trace) with an increase in the cathodic current up to 20 h of measurement. Lange et al. [15] have already reported a similar increase in the cathodic current measured at 0 V/MSE, a potential in the autocatalytic region for the nitric acid reduction on a gold microelectrode in 8 mol L^{-1} HNO_3 at RT. These authors suggested that the observed plateau was due to $NO_{(ads)}$ desorption, considered the determining step during the autocatalytic cycle. Additionally, a careful analysis of the sample surface (using optical microscopy and profilometry) after the experiment performed at 107 °C did not show any significant change that could be at the origin of the increase in the cathodic current by about two orders of magnitude after 20 h of measurement. The boiling solution may also influence the reduction reaction by creating a hydrodynamic regime different from that of a non-boiling solution and resulting in different evolution of the system with respect to the build-up of reaction products near the electrode surface.

3.1.2. EIS measurements

EIS measurements were successively performed after each chronoamperometry experiment at the corresponding potential. **Figure 4** shows the Nyquist representation of the spectra obtained for four temperatures (40, 60, 80 and 107 °C). For each panel, the black symbols correspond to the measurements performed at the corrosion potential.

At 40 °C (**Figure 4**a), the charge transfer resistance, R_{ct}, obtained from the diameter of the high-frequency capacitive loop, decreases with the cathodic overpotential. Below -0.3 V/MSE, a significant decrease of R_{ct} is observed concomitantly with an increase in the cathodic current densities in this potential range. At -0.4 V/MSE, a second time constant in the low-frequency domain, an inductive loop, starts to be observed. This time constant could reveal a mechanism involving the relaxation of adsorbed species onto the electrode surface and could be attributed to the autocatalytic reduction of nitric acid, as previously mentioned. Interestingly, this agrees well with the Balbaud et al.'s work stating that the reduction of nitric acid on a 304L stainless steel alloy requires higher overpotentials for the Schmid mechanism [21].

The high-frequency capacitive loop is still observed at higher temperatures (**Figure 4**b-d). Still, at the corrosion potential, the characteristic frequency increases and the charge transfer resistance decreases as the temperature increases, in agreement with faster kinetics at higher temperatures. Moreover, the second time constant (i.e., the low-frequency inductive loop) can be observed at -0.3 and -0.4 V/MSE.

At 107 °C, the change in kinetics is expressed by the presence of two capacitive time constants (**Figure 4**d) that, in low-frequency, progressively transform into an inductive time constant when the potential decreases. Such behaviour can be observed in the case of a mechanism involving an adsorbed intermediate [25].

As previously explained, the reduction reaction of nitric acid is amplified for sufficiently low potentials in the vicinity of the active domain (i.e., dissolution of the stainless-steel material). If the active domain is set to that required for the autocatalytic regime, the reduction kinetics will be exalted, and the oxide layer will no longer play its passivating role, thus enhancing the electron exchange at the metal/solution interface. Such a situation is likely at high

temperatures (80 and 107 °C) for which the reaction kinetics is increased, justifying the temperature range selected in the following analytical study for the reduction by nitric acid on silicon-enriched stainless steel. At this stage, the analysis of EIS diagrams was only performed from a qualitative point of view, since any attempt in using electrical equivalent circuit would be compromised because of the complexity of the system, and in the following of the paper, we will mainly focus on the identification of the main species and reaction steps.

3.2. Identification of the species involved in the nitric acid reduction mechanism on stainless steel

3.3.1 Role of Fe(III) and HNO_2 in the reduction mechanism

Electrochemical measurements can also help distinguish between anodic and cathodic reactions on stainless steel. The building up of non-negligible amounts of corrosion products in solution must be considered for long-time exposure of stainless steel to concentrated nitric acid. In a recent study, Pellé et al. reported on the catalytic role of the Fe(III) ions in the reduction of concentrated nitric acid (4 mol L^{-1}) at 40 °C on a gold electrode [26]. For this reason, the Fe(III) concentration was determined during cathodic polarization using ICP-AES analyses. In addition, nitrous acid concentration was also monitored, as this species is thought to play a major role in the reduction mechanism of nitric acid in solution [13–15,21,26].

Figure 5 shows the current density evolution during successive modifications of the cathodic potential (-0.45 V/MSE, -0.6 V/MSE and -0.45 V/MSE) on the stainless steel electrode at 80 and 107 °C. Solution sampling was performed during the measurements to monitor the evolution of the Fe(III) and HNO_2 concentrations over time, which changes are overlaid on the same plots. The switch back to -0.45 V/MSE after applying -0.6 V/MSE for several hours (i.e., a cathodic potential in the active region) was aimed at checking the impact of a rapid build-up of corrosion products in the solution. If Fe(III) ions are present in solution in sufficient quantity to catalyse the nitric acid reduction reaction after 15-20 h of polarisation at

-0.6 V/MSE, then the current generated at -0.45 V/MSE afterwards should be larger compared to that recorded within the first exposure to this potential.

At 80 °C (**Figure 5a**), a clear correlation can be observed between the evolution of the concentration of HNO_2 and the cathodic current density. When a quasi-steady-state current is achieved, for a given potential, the HNO_2 concentration remains essentially constant until the potential is set to a different value. The reduction reaction is exalted when a potential of -0.6 V/MSE, corresponding to a potential in the active domain, is applied. In this case, the oxide layer should be less protective, which enhances electron exchanges. HNO_2 reaches a very high concentration (about 10^{-2} mol L^{-1}, the interfacial concentration being probably larger), which tends to turn the solution yellow in the reactor. When -0.45 V/MSE is newly applied, the HNO_2 concentration decreases together with the current density. At such an applied potential, the current density slowly evolves towards a steady-state value of about -0.5 mA cm^{-2}, which is close to the initial current density of about -0.2 mA cm^{-2}. This indicates that no significant influence of the Fe(III) ions accumulated in the solution is observed. After 20 h at -0.6 V/MSE, about 4.5 x 10^{-5} mol L^{-1} of Fe(III) appears in the solution. This concentration may not be sufficient to contribute to the autocatalysis reaction compared to that of 5 x 10^{-2} mol L^{-1} reported by Pellé et al. [26]. As the Fe(III) concentration in the present study remains far from that required for autocatalysis [26], establishing the autocatalysis reaction should essentially depend on the nitrogen species involved in the reduction reaction. This conclusion is also consistent with the work of Balbaud et al., who investigated the reduction of nitric acid on a 304L stainless steel alloy [21].

At 107 °C (**Figure 5**b), similar behaviour is observed, except that HNO_2 is present in a much lower concentration compared to the experiment performed at 80 °C due to the boiling regime, which likely leads to the release of HNO_2 in the gas phase and an increase in the NO_x production according to the following equation:

$$2HNO_{2\,(aq)} \longleftrightarrow NO_{2\,(aq)} + NO_{(aq)} + H_2O_{(l)} \qquad (12)$$

The quantification of HNO_2 at 107 °C was therefore not always possible as its concentration most often fell below the detection limit of the analytic technique (< 10^{-6} mol L^{-1}). Nonetheless, an increase in nitrous acid concentration could be recorded after 18 h of polarization at -0.6 V/MSE (active domain potential). This indicates that the build-up of HNO_2 in the solution appears to be possible when its production from the reduction reaction becomes faster than its decomposition rate at the boiling temperature (~ 4.5 x 10^{-5} mol L^{-1} after 18 h at -0.6 V/MSE). Furthermore, high cathodic current densities were measured despite the low concentration of HNO_2 in solution. This probably does not indicate that such a species is not involved in the autocatalytic reduction cycle, but rather that HNO_2 produced during the reaction is mainly transformed in NO_x species (Eq. *(12)*). The Fe(III) concentration in the solution was found to increase by a factor of 3 after applying a potential of -0.6 V/MSE, which corresponds to a concentration of 1.6 x 10^{-5} mol L^{-1}. Such a low Fe(III) concentration appears to have hardly any influence on the current density when the potential is switched to -0.45 V/MSE as the current density rapidly decreases to that recorded during the first polarization step at this potential (~2 mA cm^{-2}). In addition, the current density measured at -0.6 V/MSE at 80 °C (**Figure 5**a) was surprisingly higher than that recorded at 107 °C (**Figure 5**b). Here again, the concentration of Fe(III) ions and its dissolution rate is almost four times larger than that recorded at 107 °C. This observation is also consistent with the negligible effect of Fe(III) ions on the reduction reaction under our experimental conditions, leading to the conclusion that the autocatalytic mechanism in the nitric acid reduction should essentially result from the NO_x products stored in the solution.

3.3.2 Identification of the NO_x species involved in nitric reduction mechanism

On gold electrodes in 4 mol L^{-1} nitric acid at 40 °C, Sicsic et al. [13] and Pellé et al. [26] ascribed the production of NO_x species (NO, NO_2) to the Schmid autocatalytic mechanism. By coupling electrochemical measurement with mass spectrometry, Pellé et al. detected NO_x species released in the gas phase while applying a cathodic overpotential [26]. In this earlier study, it is important to notice that NO_x species detection in the gas phase could be achieved because of the effect of Fe(III) present in a sufficiently high concentration in the acidic solution [26] and the high reactivity of a noble metal (i.e., without a passivating film slowing down the electron transfer reaction) [13]. To our knowledge, such analyses have never been performed on a stainless-steel electrode. Furthermore, the cathodic reaction rates were reported to be three to four orders of magnitude lower than those recorded on an inert electrode made of noble metal [19].

Figure 6 shows the evolution of the ionic currents associated with the detection of NO, N_2O and NO_2 species released in the gas phase when the stainless-steel electrode was submitted to successive potentials from -0.2 to -0.6 V/MSE in a concentrated nitric acid solution at 80 °C.

Despite bubbling was observed on the stainless-steel electrode after switching from -0.2 V/MSE to a potential as high as -0.45 V/MSE in a concentrated nitric acid solution at 80 °C, the release of NO, N_2O and NO_2 in the gas phase could not be recorded by mass spectrometry (**Figure 6**a). In contrast, the ionic currents associated with the detection of NO, N_2O and NO_2 species increased to a significant extent when the potential of the stainless-steel electrode was set to -0.6 V/MSE (**Figure 6**b), which attested to releasing of such nitrogen oxide species in the gas phase under these conditions. In this figure, the changes in signal intensity indicated by the black arrows are due to the period within which sampling of the solution was performed.

Contrary to what could be observed at 80 °C, bubbling onto the stainless-steel electrode could not be unequivocally ascertained at 107 °C because of the boiling of the nitric acid solution at

such a temperature. When similar measurements were carried out on the stainless steel electrode at 107 °C, a temperature at which the kinetics of nitric acid reduction is known to be faster and the solubility of gases to be lower compared to those at lower temperatures, an increase in the ionic currents related to the NO and NO_2 gas phase species appeared to be observed when a sufficient potential of -0.45 V/MSE was applied to the stainless steel electrode (no gas production was detected at the previously applied potentials of -0.3 and -

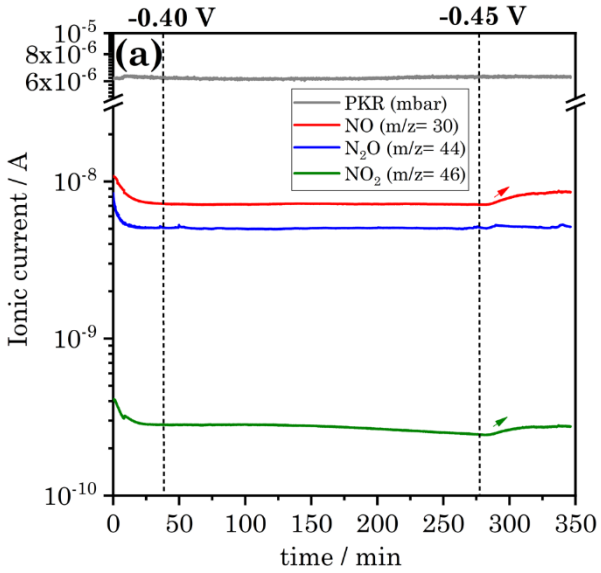

0.40 V/MSE) (

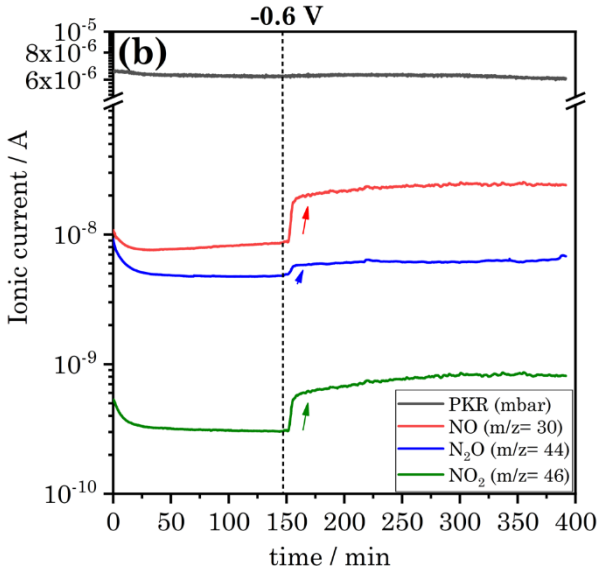

Figure 7a). These latter ionic currents were found to be promoted with an applied potential of -0.6 V/MSE, and that related to N_2O could be observed (

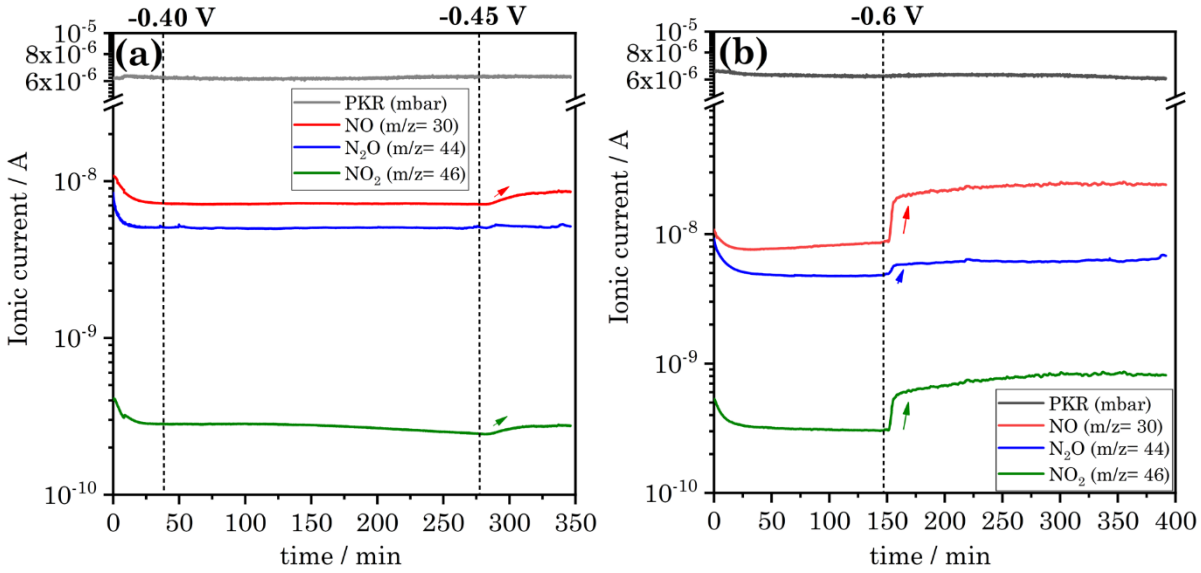

Figure 7b). The comparison of the ionic currents related to the release of nitrogen oxide species in the gas phase, recorded with a potential of -0.6 V/MSE applied to the stainless steel electrode at various temperatures (**Figure 6** and

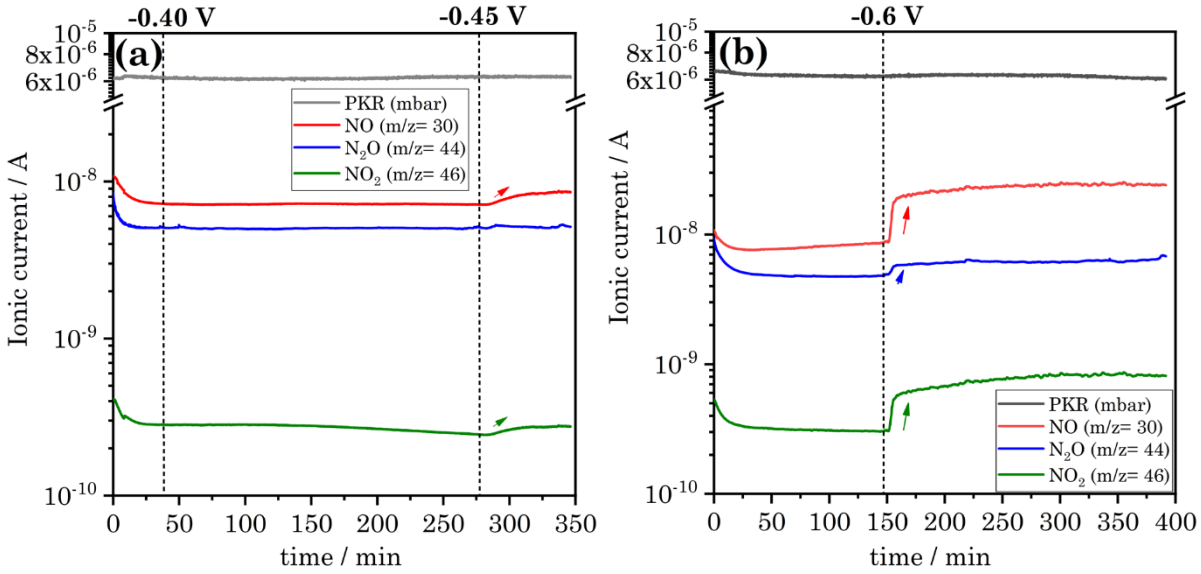

Figure 7b), suggests that higher amounts of NO and NO_2, and lower amounts of N_2O were released in the experiment performed at 107 °C compared to that performed at 80 °C. At both

temperatures, changes in the releases of NO and NO_2 appears to be correlated (**Figure 6** and

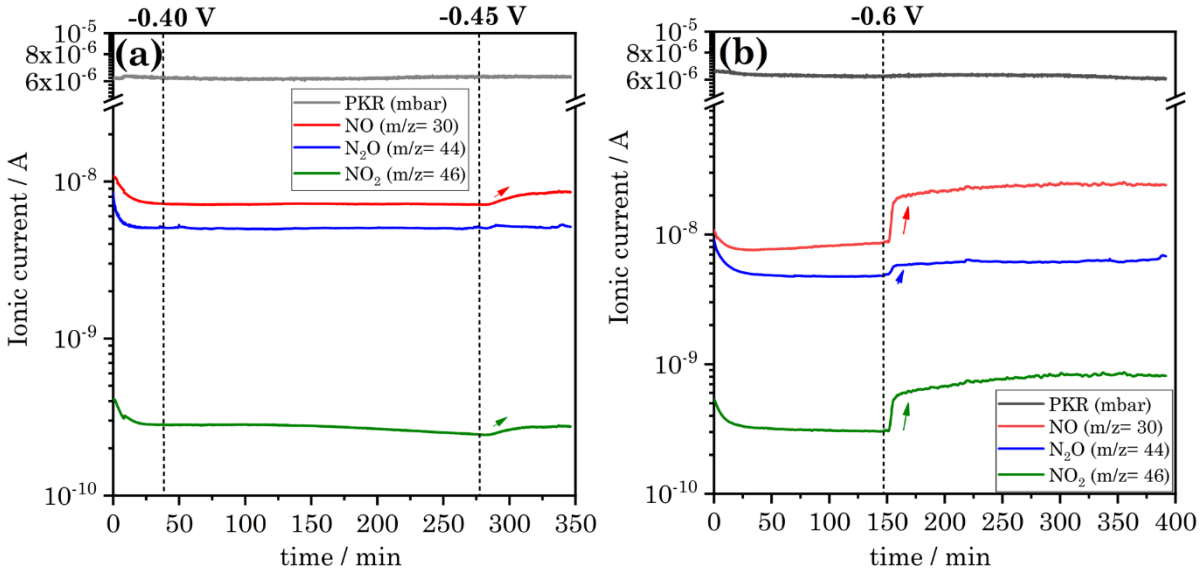

Figure 7). The presence of N_2O must result from the NO reduction reaction (Eq. *(11)*), which takes place with the cathodic overpotential in parallel to the autocatalytic cycle.

3.3.3 Towards a global understanding of nitric acid reduction on Si-enriched stainless steel

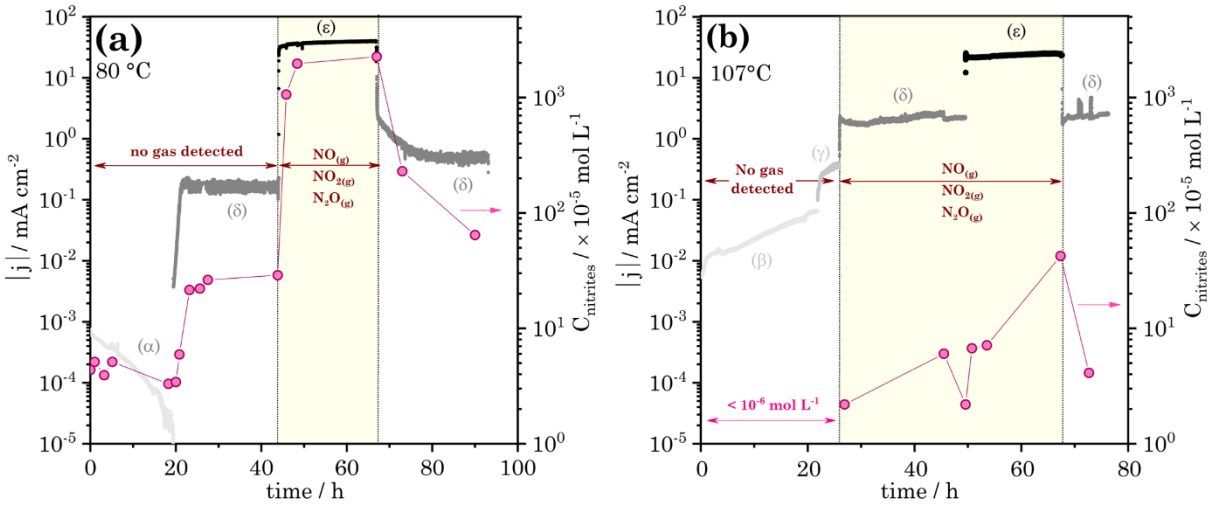

Figure 8 summarizes the analytical study performed with the EC-MS set-up and the analysis of the production of gaseous nitrogen oxide species over a broad cathodic potential domain (between E_{corr} and -0.6 V/MSE) at 80 and 107 °C. The domains of potential denoted as δ and ε in

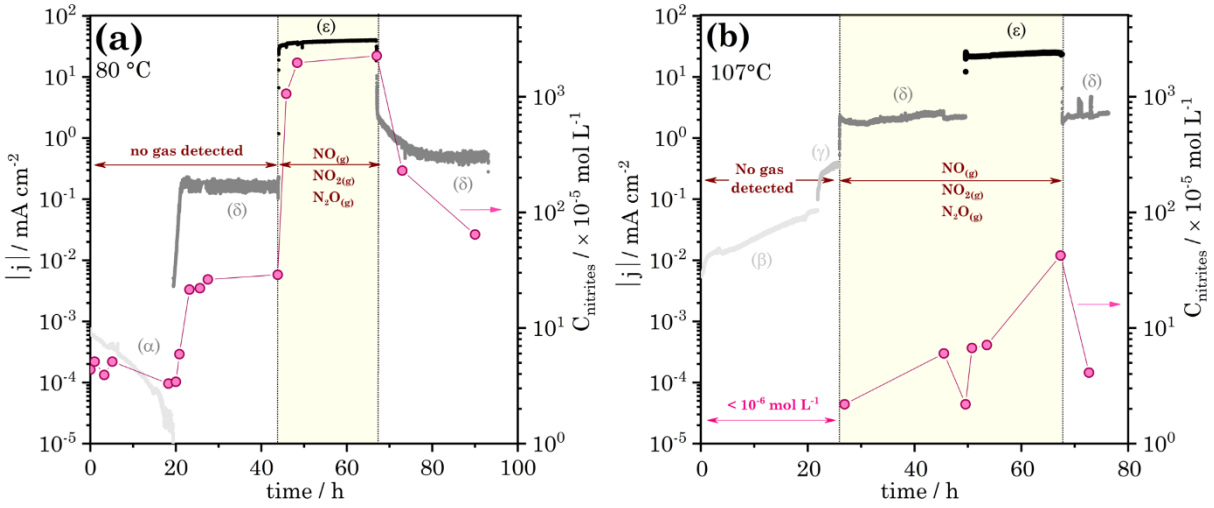

Figure 8 correspond to those already shown in **Figure 5**. The experiment performed at 80 °C allows asserting that HNO_2 is associated with the current evolution. Meanwhile, the experiment carried out at 107 °C permits to detect of NO_x species in the gas phase from a potential as high as -0.45 V/MSE. Such a high potential can be due to several factors: an

earlier transition active/passive domain that accelerates faradaic reactions, a facilitated release of NO_x species in the gas phase with the boiling regime and a faster kinetics of the nitric acid reduction reaction due to the higher temperature of the medium.

At -0.6 V/MSE, the stainless-steel electrode does not have a passivating oxide layer, as the potential belongs to the active domain of the material. In this configuration, NO_x species and nitrous acid are produced for both temperatures.

Above -0.45 V/MSE, the current generated is not sufficient to overcome the detection limit of gas analysis. According to EIS and chronoamperometry analyses, the mechanism that allows the formation of HNO_2 and NO_x gaseous species starts to be activated at -0.3 V/MSE. This mechanism would involve NO_x adsorbed species intermediates such as $NO_{(ads)}$, whereas the Fe(III) ion produced by the dissolution of stainless steel shows no significant effect on this mechanism.

4. Conclusions

This study puts particular emphasis on the complexity of the nitric acid system. As expected, cathodic currents are increased mainly by the temperature. The same reduction mechanism seems to occur at the electrode in the studied temperature range. Therefore, the temperature would mostly play a role in the kinetics of nitric acid reduction. Below -0.3 V/MSE, an autocatalytic mechanism involving nitrogen oxide adsorbed species and reduction products such as nitrous acid and NO_x gaseous species has been consistently demonstrated with a Schmid's type mechanism. The active domain of stainless steel can amplify the reduction reaction as the electron exchange is facilitated due to the absence or the decrease in thickness of the passivating film. The latter has no specific role in the autocatalytic cycle except that its insulating properties, depending on the potential of the stainless steel, can slow down the

autocatalytic cycle. Yet, the low detection of HNO_2 in solution at the boiling temperature (107 °C) does not prevent the occurrence of the autocatalytic cycle, which can be accounted for by the liquid/gas equilibria that are amplified in boiling conditions.

Acknowledgments

Authors are grateful to Orano for its financial support.

Figures

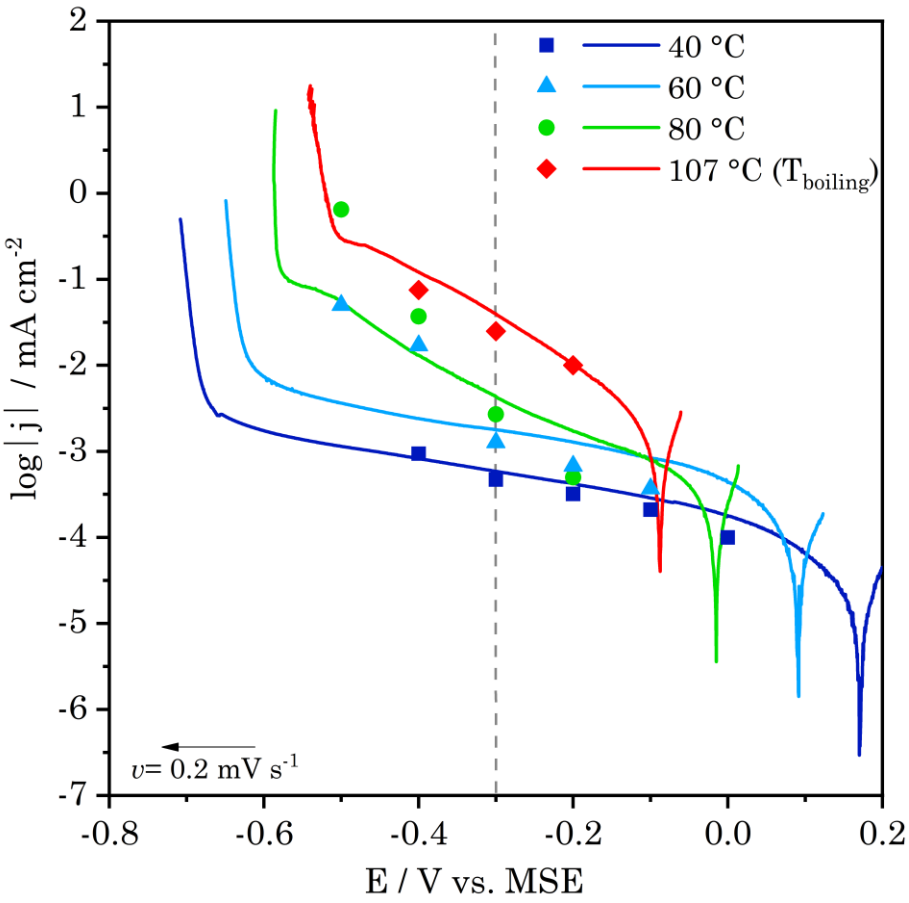

Figure 1. Linear sweep voltammetry at v = 0.2 mV s^{-1} (coloured lines) and steady-state current density measured at various potentials (symbols) for the X1 Cr-Ni-Si 18-15-4 electrode in 2.5 mol L^{-1} HNO_3 + 2.5 mol L^{-1} $NaNO_3$ at 40 °C (blue trace), 60 °C (light-blue trace), 80 °C (green trace) and 107 °C (red trace). The vertical dash line at -0.3 V/MSE indicates the beginning of the potential region of the autocatalytic mechanism of nitric acid reduction.

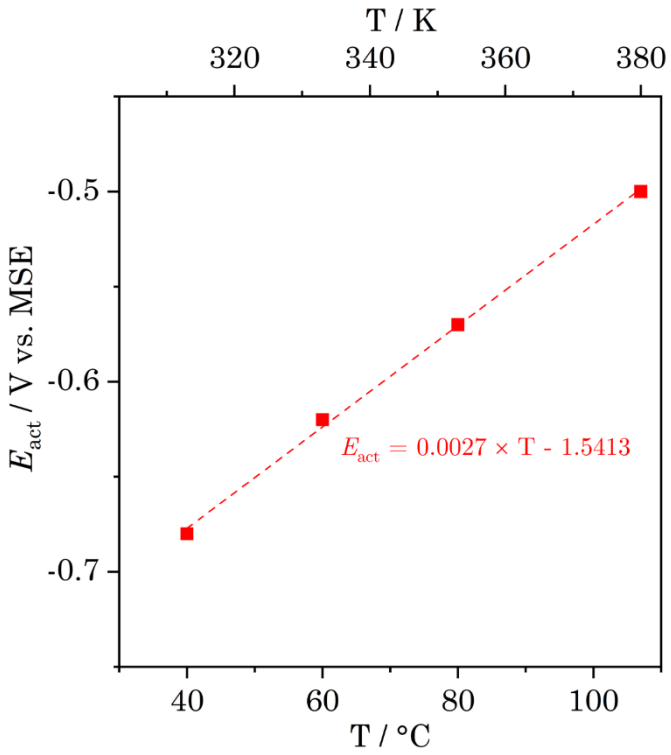

Figure 2. Evolution of the active/passive transition potential, E_{act}, of the silicon-enriched stainless steel electrode as a function of the temperature determined from the data displayed in **Figure 1**.

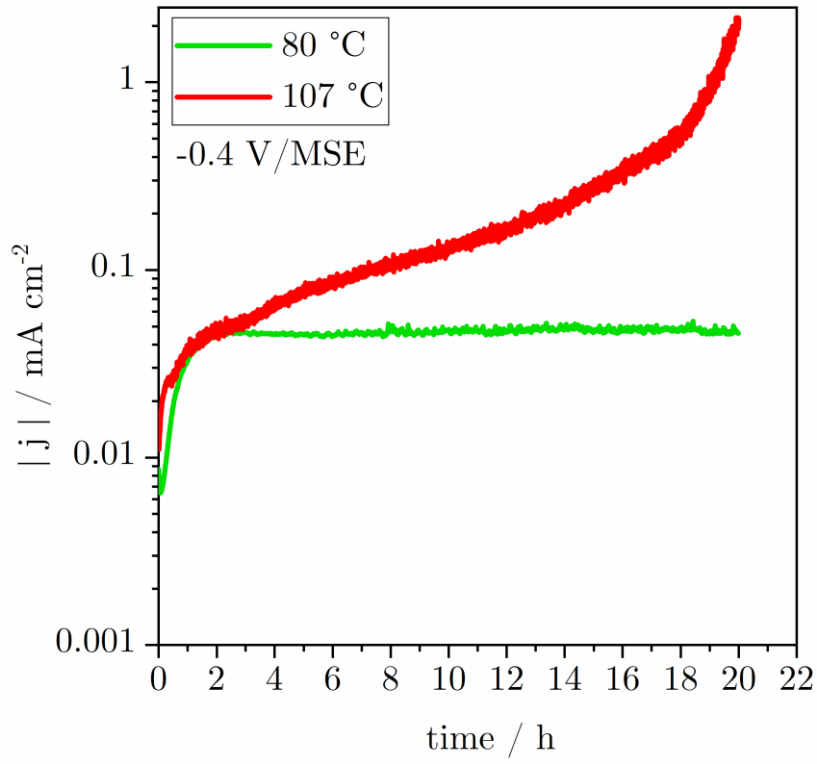

Figure 3. Evolution of the cathodic current as a function of time for a chronoamperometry experiment performed at -0.4 V/MSE in a 2.5 mol L^{-1} HNO_3 + 2.5 mol L^{-1} $NaNO_3$ solution at 80 °C (green trace) and 107 °C (red trace) on the X1 Cr-Ni-Si 18-15-4 electrode.

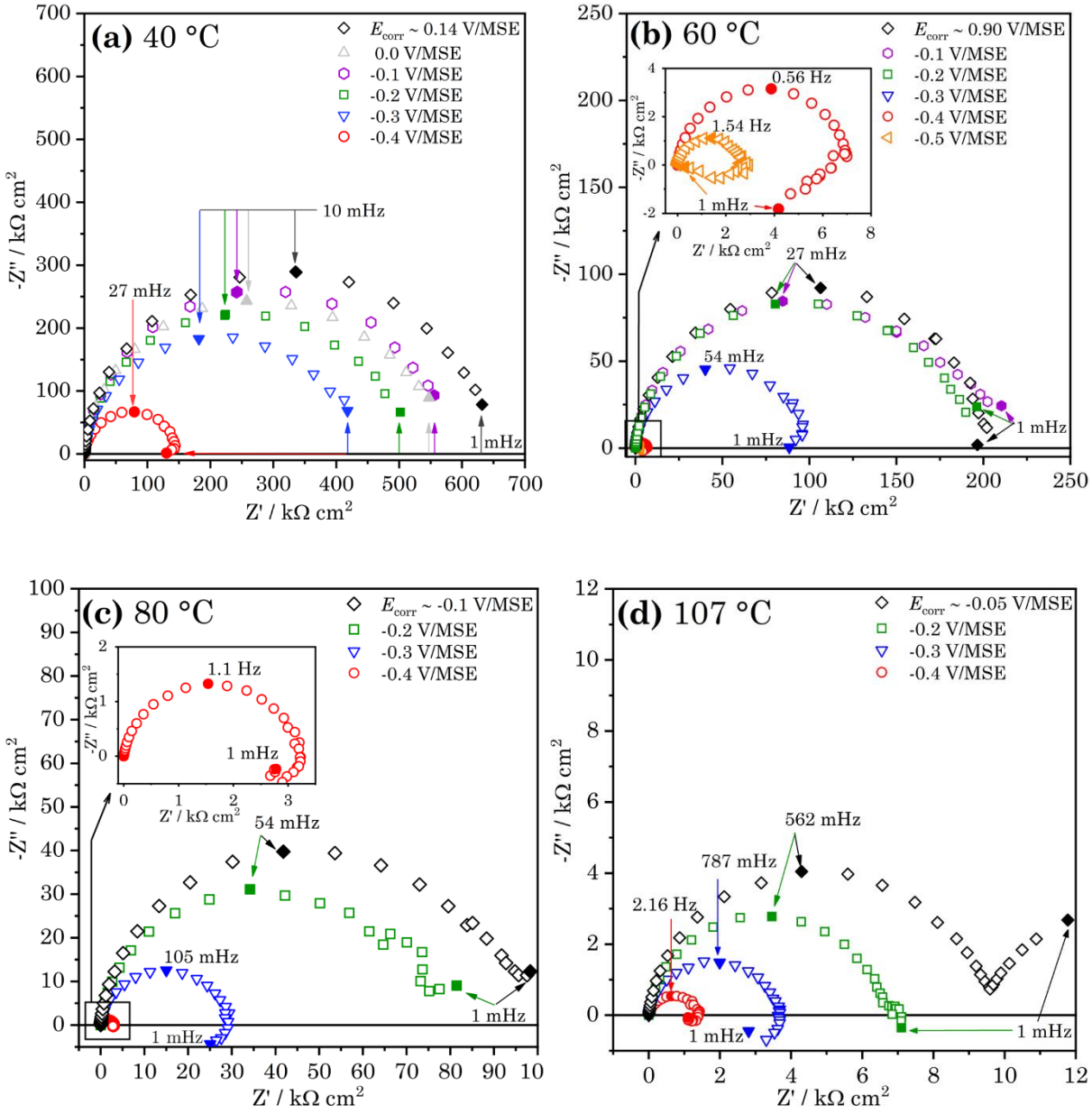

Figure 4. Nyquist representation of the EIS measurements at different cathodic potentials in a 2.5 mol L^{-1} HNO_3 + 2.5 mol L^{-1} $NaNO_3$ solution at: (a) 40, (b) 60, (c) 80 and (d) 107 °C

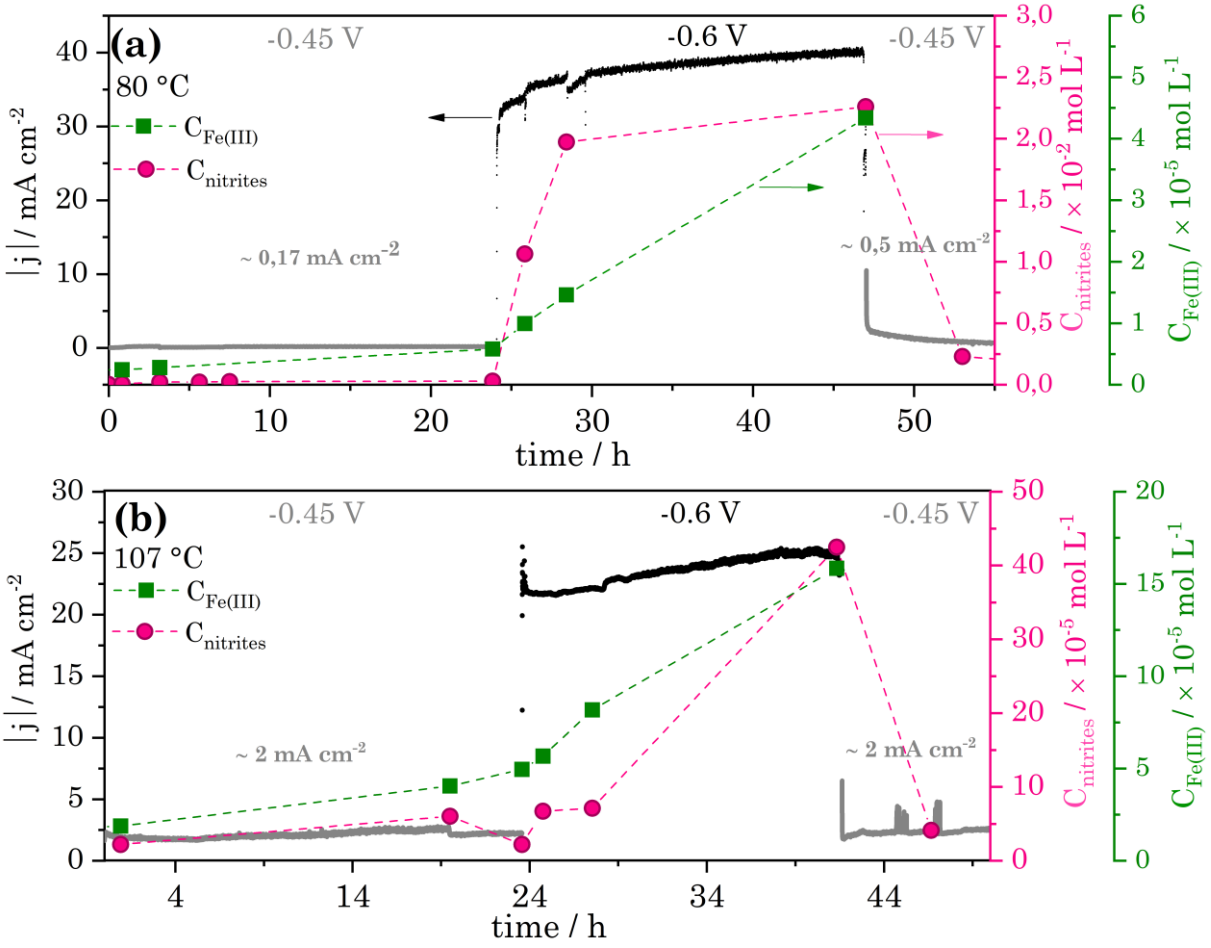

Figure 5: Evolution of the current density, and the nitrites and Fe(III) concentrations as a function of time while applying successively -0.45 V/MSE, -0.6 V/MSE and -0.45 V/MSE at 80 °C (a) and 107 °C (b) in the 2.5 mol L^{-1} HNO_3 + 2.5 mol L^{-1} $NaNO_3$ solution.

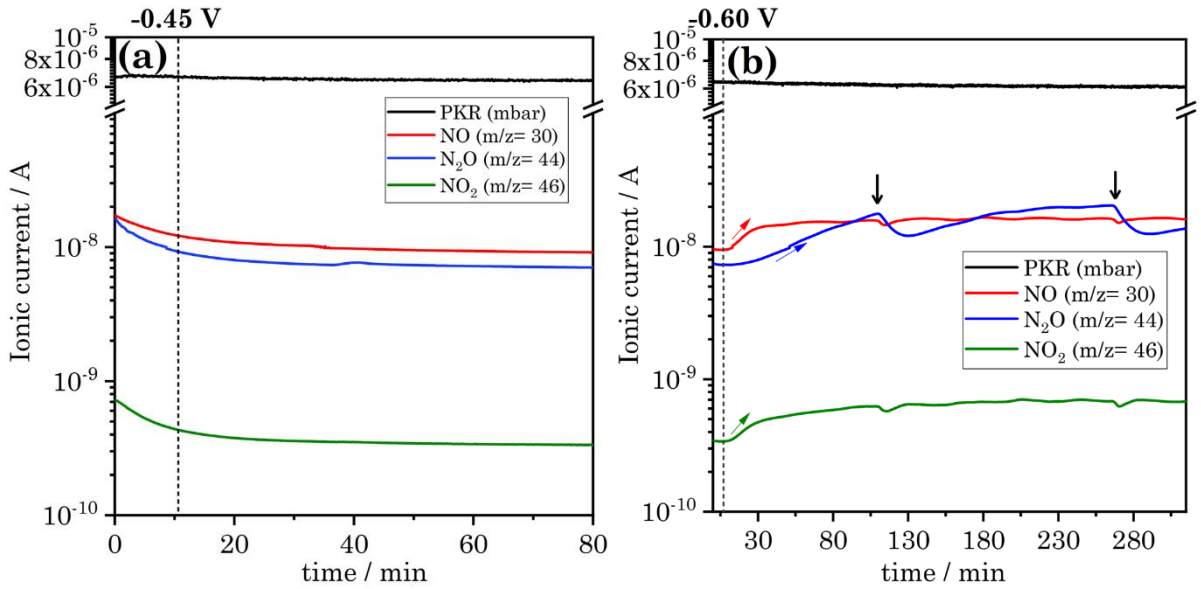

Figure 6. Evolution of the ionic currents corresponding to the NO, N_2O and NO_2 species released in the gas phase as a function of time on the stainless steel electrode in the 2.5 mol L^{-1} HNO_3 + 2.5 mol L^{-1} solution at 80 °C after applying potentials: (a) from -0.2 to -0.45 V/MSE and (b) from 0.45 to -0.6 V/MSE. The total ionic current, directly related to the pressure in the mass spectrometer, is also shown and denoted as PKR (mbar).

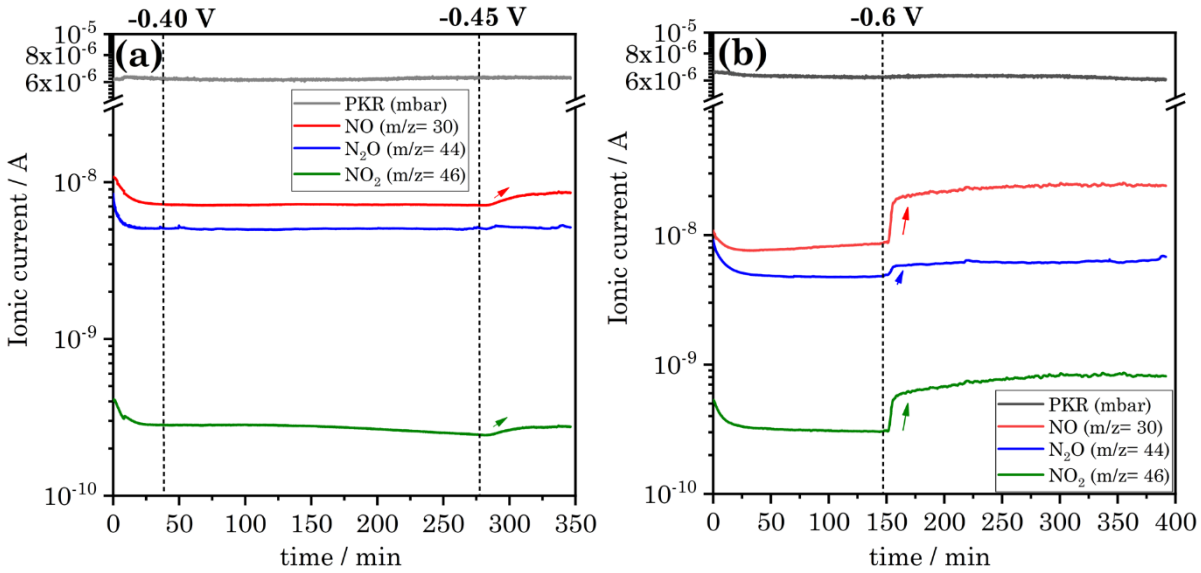

Figure 7. Evolution of the ionic currents corresponding to the NO, N_2O and NO_2 species released in the gas phase as a function of time on the stainless steel electrode in the 2.5 mol L^{-1} HNO_3 + 2.5 mol L^{-1} solution at 107 °C after applying potentials: (a) from -0.3 to -0.4 and -0.45 V/MSE and (b) from -0.45 to -0.6 V/MSE. The total ionic current, directly related to the pressure in the mass spectrometer, is also shown and denoted as PKR (mbar).

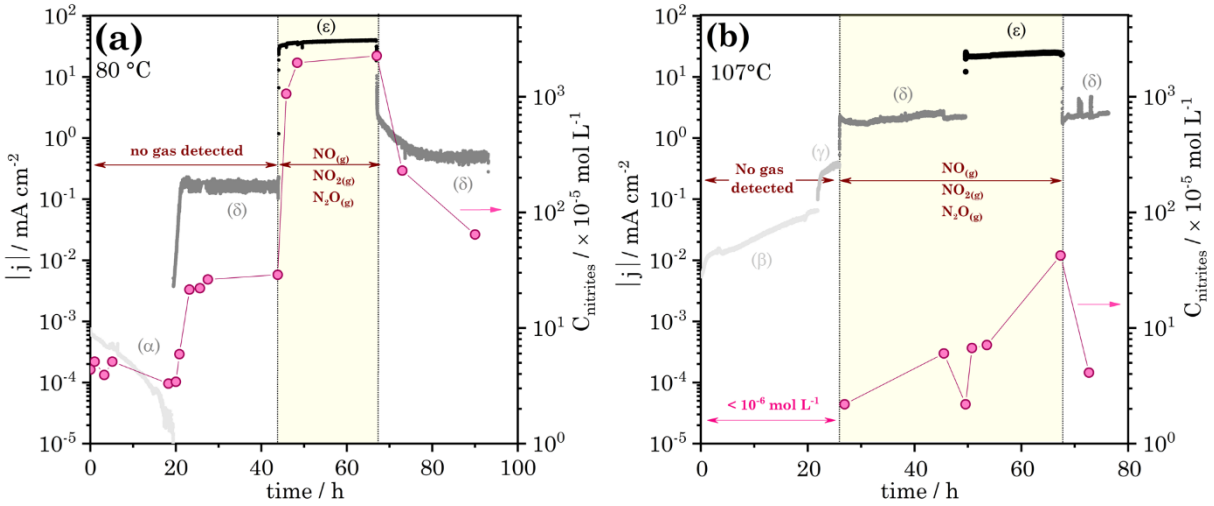

Figure 8: *(left y-axis):* Evolution of the cathodic current density as a function of time for various applied potentials at (a) 80 °C : (α) -0.2 V/MSE, (δ) -0.45 V/MSE (ε) -0.6 V/MSE V/MSE and (b) 107 °C: (β) -0.3 V/MSE, (γ) -0.4 V/MSE, (δ) -0.45 V/MSE, (ε) -0.6 V/MSE, (δ) -0.45 V/MSE; *(right y-axis):* Nitrites concentration measured in solution and represented with pink circles.

References

[1] I.D. Rosca, F. Watari, M. Uo, T. Akasaka, Oxidation of multiwalled carbon nanotubes by nitric acid, Carbon. 43 (2005) 3124–3131.

[2] L. Stobinski, B. Lesiak, L. Kövér, J. Tóth, S. Biniak, G. Trykowski, J. Judek, Multiwall carbon nanotubes purification and oxidation by nitric acid studied by the FTIR and electron spectroscopy methods, Journal of Alloys and Compounds. 501 (2010) 77–84.

[3] E.P. Nardi, F.S. Evangelista, L. Tormen, T.D. Saint´Pierre, A.J. Curtius, S.S. de Souza, F. Barbosa, The use of inductively coupled plasma mass spectrometry (ICP-MS) for the determination of toxic and essential elements in different types of food samples, Food Chemistry. 112 (2009) 727–732.

[4] M. Miguirditchian, V. Vanel, C. Marie, V. Pacary, M.-C. Charbonnel, L. Berthon, X. Hérès, M. Montuir, C. Sorel, M.-J. Bollesteros, S. Costenoble, C. Rostaing, M. Masson, C. Poinssot, Americium Recovery from Highly Active PUREX Raffinate by Solvent Extraction: The EXAm Process. A Review of 10 Years of R&D, Solvent Extraction and Ion Exchange. 38 (2020) 365–387.

[5] R.D. Armstrong, G.E. Cleland, G.O.H. Whillock, Effect of dissolved chromium species on the corrosion of stainless steel in nitric acid, Journal of Applied Electrochemistry. 28 (1998) 1205–1211.

[6] E.M. Horn, Effects of temperature and concentration on the corrosion of austenitic stainless steels in nitric acid, Metalurgia I Odlewnictwo. 16 (1990) 189–201.

[7] G. Schmid, J. Delfs, Die autokatalytische Natur der kathodischen Reduktion von Salpetersäure zu salpetriger Säure II. Der galvanostatische Einschaltvorgang, Zeitschrift für Elektrochemie, Berichte der Bunsengesellschaft für physikalische Chemie. 63 (1959) 1192–1197.

[8] G. Schmid, Die autokatalytische Natur der kathodischen Reduktion von Salpetersäure zu salpetriger Säure: III Mathematische Behandlung einer autokatalytischen Elektrodenreaktion 1. Ordnung, Zeitschrift für Elektrochemie, Berichte der Bunsengesellschaft für physikalische Chemie. 65 (1961) 531–534.

[9] G. Schmid, G. Krichel, Die autokatalytische Natur der kathodischen Reduktion von Salpetersäure zu salpetriger Säure IV. Der potentiostatische Einschaltvorgang [1], Berichte der Bunsengesellschaft für physikalische Chemie. 68 (1964) 677–688.

[10] K.J. Vetter, Entgegnung auf die vorstehende Arbeit von G. Schmid über "Die autokatalytische Natur der kathodischen Reduktion von Salpetersäure zu salpetriger Säure," Zeitschrift für Elektrochemie. 63 (1959) 1189–1191.

[11] V.P. Razygraev, M.V. Lebedeva, S.A. Kabakchi, E.Y. Ponomareva, R.S. Balovneva, L.P. Lobanova, Features of cathode reduction of boiling solutions of nitric acid on a platinum electrode, J. Appl. Chem. USSR. 61 (1988) 71–79.

[12] V.P. Razygraev, M.V. Lebedeva, S.A. Kabakchi, Certain characteristics of the cathodic reduction of nitric acid on a platinum electrode, Dokl. Phys. Chem. 288 (1986) 4–6.

[13] D. Sicsic, F. Balbaud-Célérier, B. Tribollet, Mechanism of Nitric Acid Reduction and Kinetic Modelling, Eur. J. Inorg. Chem. (2014) 6174–6184.

[14] F. Balbaud Celerier, G. Sanchez, G. Santarini, G. Picard, Cathodic Reactions Involved in Corrosion Processes Occurring in Concentrated Nitric Acid at 100 °C, Eur. J. Inorg. Chem. 2000 (2000) 665–674.

[15] R. Lange, E. Maisonhaute, R. Robin, V. Vivier, On the kinetics of the nitrate reduction in concentrated nitric acid, Electrochemistry Communications. 29 (2013) 25–28.

[16] K.J. Vetter, Uber den enstellungsmechanismus des HNO2/HNO3 redoxpotentials, Z. Phys. Chem. (1950) 199–206.

[17] C. Kato, K. Kiuchi, K. Sugimoto, Thermodynamic Study on Redox Reactions of Boiling Nitric Acid Solutions, Corrosion Engineering. 52 (2003) 44–52.

[18] V. Razygraev, R.S. Balovneva, M.V. Lebedeva, E.Y. Ponomareva, Kinetics of the reduction of nitric acid on stainless steels and alloys, Protection of Metals (English Translation of Zaschita Metallov). 26 (1990) 43–48.

[19] V.P. Razygraev, M.V. Lebedeva, The effect of cathode material on nitric acid reduction kinetics, Protection of Metals and Physical Chemistry of Surfaces. 50 (2014) 833–840.

[20] M. Benoit, Modélisation de la cinétique de réduction de l'acide nitrique concentré sur acier inoxydable 304L, Ph.D. Thesis, Université Pierre et Marie Curie, 2016.

[21] F. Balbaud, G. Sanchez, P. Fauvet, G. Santarini, G. Picard, Mechanism of corrosion of AISI 304L stainless steel in the presence of nitric acid condensates, Corrosion Science. 42 (2000) 1685–1707.

[22] M.E. Orazem, B. Tribollet, Electrochemical impedance spectroscopy, Wiley, Hoboken, N.J, 2008.

[23] S. Hasegawa, Effect of boiling phenomena on the corrosion of stainless steel (R-SUS304ULC) in nitric acid solution containing chromium ions, Paper presented at 23rd International Conference on Nuclear Engineering: Nuclear Power - Reliable Global Energy, ICONE 2015, Chiba, Japan, 2015.

[24] B. Laurent, Compréhension du comportement en corrosion d'un acier austénitique inoxydable enrichi en silicium en milieu acide nitrique chaud et concentré, Ph.D. Thesis, Université de recherche Paris Sciences et Lettres, 2017.

[25] C. Gabrielli, Identification of Electrochemical Processes by Frequency Response, Solartran Instrumentation Group Monograph 004/83, 1984.

[26] J. Pellé, N. Gruet, B. Gwinner, M.L. Schlegel, V. Vivier, On the role of Fe(III) ions on the reduction mechanisms of concentrated nitric acid, Electrochimica Acta. 335 (2020) 135578.